Nanoscale

ROYAL SOCIETY OF CHEMISTRY

COMMUNICATION

View Article Online
View Journal | View Issue

Check for updates

Cite this: *Nanoscale*, 2023, **15**, 16268

Received 30th July 2023,
Accepted 1st October 2023

DOI: 10.1039/d3nr03744d

rsc.li/nanoscale

Published on 02 Nhlangula 2023. Downloaded on 2025-09-02 21:37:52.

Magnetically locked Janus particle clusters with orientation-dependent motion in AC electric fields†

Jin Gyun Lee, ‡ Cooper P. Thome, ‡ Zoe A. Cruse, Arkava Ganguly, Ankur Gupta and C. Wyatt Shields, IV *

Active particles, or micromotors, locally dissipate energy to drive locomotion at small length scales. The type of trajectory is generally fixed and dictated by the geometry and composition of the particle, which can be challenging to tune using conventional fabrication procedures. Here, we report a simple, bottom-up method to magnetically assemble gold-coated polystyrene Janus particles into "locked" clusters that display diverse trajectories when stimulated by AC electric fields. The orientation of particles within each cluster gives rise to distinct modes of locomotion, including translational, rotational, trochoidal, helical, and orbital. We model this system using a simplified rigid beads model and demonstrate qualitative agreement between the predicted and experimentally observed cluster trajectories. Overall, this system provides a facile means to scalably create micromotors with a range of well-defined motions from discrete building blocks.

Department of Chemical and Biological Engineering, University of Colorado Boulder, Boulder, CO 80303, USA. E-mail: Charles.Shields@colorado.edu

†Electronic supplementary information (ESI) available: Experimental details, details on the ICEP propulsion chamber, details on the beads model. See DOI: https://doi.org/10.1039/d3nr03744d

‡These authors contributed equally to this work.

C. Wyatt Shields IV

C. Wyatt Shields IV is currently an Assistant Professor in the Department of Chemical and Biological Engineering at the University of Colorado Boulder. He received his B.S. from the University of Virginia in 2011 and Ph.D. from Duke University in 2016. He is a Packard Fellow in Science and Engineering, Pew Biomedical Scholar, and recipient of an NSF CAREER award, ONR YIP award, and NIH R35 MIRA. His research group is developing field-responsive and active particles as vehicles for next-generation biosensing, drug delivery, and immunoengineering.

Introduction

Micromotors composed of active colloidal particles have found use in a multitude of applications, including drug delivery,[1–4] cell manipulation,[5–7] flexible electronics,[8–10] and cargo transport.[11–15] Such micromotors can be propelled by various energy sources, including magnetic,[16–21] acoustic,[2,22–24] and electric fields,[11,25–28] as well as catalytic reactions.[29–33] As a category of electrical stimulation, induced-charge electrophoresis (ICEP) is a useful method to drive the motion of metallodielectric particles (*e.g.*, dielectric particles with metal patches) in alternating current (AC) electric fields due to the highly tunable interactions between the particles and applied field.[11,25,34–36] In the case of a metallodielectric particle undergoing ICEP, the patch geometry is a major determinant of particle locomotion;[37–40] however, the ability to control patch morphology, and thus particle trajectory, is limited.

Previous work has studied the locomotion of dimeric Janus particle clusters,[41,42] which have the capacity to exhibit nonlinear trajectories. However, this approach has only been shown to produce two regimes of locomotion (*i.e.*, linear and orbital). By assembling Janus particles (*i.e.*, spherical particles with two distinct hemispheres) into multiparticle clusters with complex relative orientations, we hypothesized that it is feasible to replicate the motion of singular Janus particles and access new regimes of motion not otherwise attainable using traditional Janus particles.

Here, we utilize a high-throughput approach to show the first demonstration of magnetically "locked" assemblies of metallodielectric Janus particles that exhibit five distinct regimes of locomotion when driven by ICEP (*i.e.*, translational, rotational, trochoidal, helical, and orbital). Four of these regimes are accessible by clusters comprising only two Janus

This journal is © The Royal Society of Chemistry 2023

Published on 02 Nhlangula 2023. Downloaded on 2025-09-02 21:37:52.

particles. By assembling Janus particles into larger clusters, such as trimers, or assembling particles with non-hemispherical patches (*i.e.*, patchy particles),[43–45] we observe a broader diversity of motions within a single experiment (*e.g.*, orbital motions of patchy–Janus particle clusters and helical motions of trimeric Janus particle clusters). To examine the relationship between particle orientations within a cluster and the resultant cluster motions, we show that a force-torque model can qualitatively predict the trajectory of assembled clusters in AC electric fields. This system provides a simple, high-throughput avenue for the study and future design of micromotors with distinct trajectories and functions, such as those that must navigate complex 3D environments to deliver cargo.

Results and discussion

In the case of metallodielectric particles, ICEP originates from asymmetric electroosmotic flows over the regions of differing polarizabilities. When a uniform AC field in the kHz frequency range is applied to a metallodielectric Janus particle within a liquid, the particle reorients such that the interface between the hemispheres aligns parallel with the field due to dielectrophoresis (DEP), yielding the greatest possible induced dipole moment.[46,47] After this reorientation, ions in solution accumulate preferentially at the surface of the metallic hemisphere, generating an induced charge cloud. At steady state, due to this induced charge cloud, fluid is drawn to the particle parallel to the field and ejected perpendicular to the field, away from the two hemispheres.[48,49] Importantly, electroosmotic flows dominate over the region of the particle that is more polarizable, resulting in asymmetric fluid flows around the particle and propulsion in the direction of the less polarizable region.[25,37,43,46,50] Thus, to fabricate non-magnetic Janus particles for this study, we used electron-beam (e-beam) evaporation to coat one hemisphere of commercial 5.1 μm fluorescent polystyrene (PS) particles with gold (Au) due to the large mismatch in the polarizability of both materials. To fab-

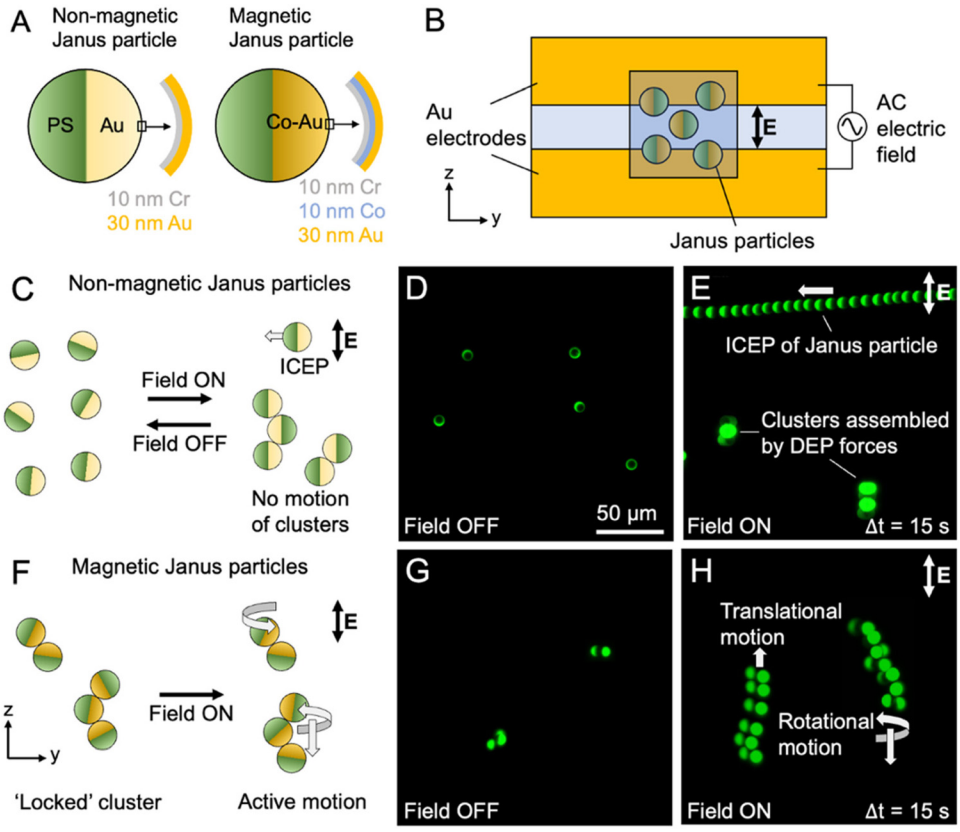

Fig. 1 Fabrication and propulsion of non-magnetic *versus* magnetically locked Janus particles in AC electric fields. (A) Schematic illustration of the preparation of Janus particles. Polystyrene spheres on a substrate are coated with Cr and Au to prepare non-magnetic Janus particles or Cr, Co, and Au to prepare magnetic Janus particles, all using e-beam evaporation. (B) Schematic representation of the coplanar electrode propulsion chamber. The particle dispersion is introduced between two gold electrodes, and a high frequency AC square wave is applied. (C) Schematic image showing propulsion and assembly of non-magnetic Janus particles in AC electric fields. Upon removal of the electric field, particles disassemble. (D) Fluorescent microscopy image showing dispersed non-magnetic particles before applying an AC electric field. (E) Superimposed fluorescent microscopy image of non-magnetic Janus particles in a uniform AC electric field. A single Janus particle propels with a linear trajectory due to ICEP, while particles assembled by dielectrophoretic forces and aligned with the electric field do not exhibit any motion. (F) Schematic illustration showing propulsion of a magnetically locked cluster of Janus particles in AC electric fields. (G) Fluorescent microscopy image showing pre-assembled magnetic particles before applying AC electric fields. (H) Superimposed fluorescent microscopy image showing propulsion of magnetic clusters.

Published on 02 Nhlangula 2023. Downloaded on 2025-09-02 21:37:52.

ricate magnetic Janus particles capable of locking into varied cluster configurations, we deposited a thin layer of cobalt (Co) – a ferromagnetic material – between the polystyrene and gold layers. For both types of particles, a chromium (Cr) layer was included between the PS and the metal patch to aid adhesion of the patch (Fig. 1A). After removal from the coating substrate, we transferred the particles to Milli-Q water, as high solution ion content suppresses ICEP, at a concentration of ~2.5×10^6 particles mL^{-1}.[39,46] We then exposed the magnetic Janus particle solution to a permanent magnet (~50 Gauss), ensuring random magnetization of the Co patches of the Janus particles.

We fabricated coplanar electrokinetic propulsion chambers by depositing 20 nm Cr and 100 nm Au on a glass slide masked with a thin strip of Kapton tape spanning the length of the slide. After metal deposition, the tape was removed to reveal two Au electrodes. We attached copper (Cu) tape to each electrode to act as electrical leads. During experiments, a hydrophobic pen was used to draw a small square outline that overlapped the two electrodes, and two pieces of polytetrafluoroethylene (PTFE) tape were placed perpendicular to the electrodes at the border of the hydrophobic boundary to act as spacers. After this, 10–20 μL of solution containing the particles was pipetted onto the slide within the hydrophobic boundary, and a coverslip was placed on top of the PTFE spacers. A square wave (4 kHz for all experiments) was applied to the chamber to generate the AC electric field (~750 V cm^{-1} for all experiments) within it (Fig. 1B and Fig. S1†).

We first evaluated chamber operation by loading a solution of non-magnetic Janus particles (*i.e.*, lacking the Co layer) into a chamber situated on a fluorescence microscope equipped with a camera. Without the AC electric field applied, particle orientations were random, though the dense gold hemispheres tended to orient toward the bottom of the chamber, toward the microscope objective, due to gravity (Fig. 1C and D). Upon applying the electric field, we noted that single particles displayed linear translation perpendicular to the applied AC electric field, which is characteristic of ICEP of spherical, metallodielectric Janus particles.[46,51] We also observed DEP-mediated clustering of some particles when in close proximity. Such clustering generally led to arrested particle motion due to alignment and coupling of the cluster with the field, which results in DEP forces dominating over ICEP forces (Fig. 1E).[52] Upon removal of the applied field, these clusters disassembled as expected.

We then examined pre-magnetically locked Janus particles in the chamber. In the absence of an applied AC electric field, we saw a diverse population of Janus particle clusters, including many dimers and trimers (Fig. 1F–H). Upon application of the field, we observed a range of motions, including translational, rotational, trochoidal, helical, and nil (arrested) motions (Fig. 1H and Fig. S2, S3†). Notably, unlike the clusters of non-magnetic Janus particles that dispersed when the applied field was removed, clusters of magnetic Janus particles retained their configurations after removal of the AC electric field, confirming their assembly is mediated by the magnetic Co layer and not by DEP forces.

To begin exploring the nature of the diverse cluster motions we observed, we analyzed a dimer configuration that exhibited linear translation without rotation. As seen in both the time-lapse images (Fig. 2A and Movie S1†) and particle trajectory plot (Fig. 2B), the particle cluster moves linearly; however, the direction of motion differs from that of a single Janus particle

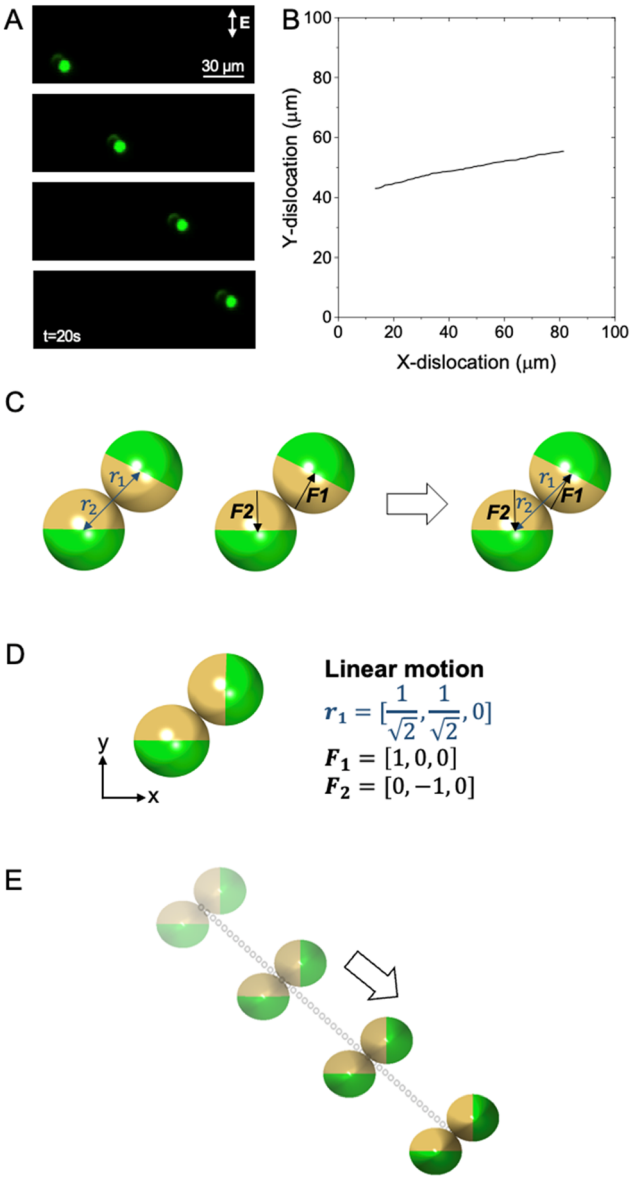

Fig. 2 Janus particle dimer exhibiting linear translational motion. (A) Time-lapse image of an experimentally observed Janus particle dimer displaying linear translation, captured *via* fluorescence microscopy. (B) Cluster trajectory, extracted from the tracking video used to create the time-lapse image in (A). (C) Schematic illustration detailing the approach for defining relative particle orientations in an assembled cluster. (D) Schematic illustration of the configuration of the dimer from (A) and the extracted approximate vectors that define the configuration. (E) Trajectory of the cluster in (D) as simulated using a rigid beads model.

 This journal is © The Royal Society of Chemistry 2023

Published on 02 Nhlangula 2023. Downloaded on 2025-09-02 21:37:52.

undergoing ICEP in that neither of the PS hemispheres directly face the direction of motion. We hypothesized that this cluster motion was a direct result of the relative orientation of the individual Janus particles. To explore this more rigorously, we defined the orientation of the two particles using a common origin (*i.e.*, the point of contact between the two particles), two position vectors, r_1 and r_2, and two force vectors, F_1 and F_2, that point from the center of the patch of each particle to its PS center (Fig. 2C and Fig. S4†). After video analysis, we determined the position vectors of the particles in the cluster to be directed along the position vectors $r_1 = [1/\sqrt{2}, 1/\sqrt{2}, 0]$ and $r_2 = [-1/\sqrt{2}, -1/\sqrt{2}, 0]$ with the point of contact designated as the origin. Notably, as r_2 is always the negative of r_1, we report only r_1 for convenience in the remainder of this discussion. The force vectors, representing the relative orientation of the metallic patches in the assembly are given by F_1 = [1,0,0] and F_2 = [0,−1,0] (Fig. 2D). We then modeled these particles by a rigid beads model where the complex forces due to asymmetric electroosmotic flow over the particles are instead modeled as a single net effective force acting normal to the center of each magnetic patch (additional information available in the "Janus assembly propulsion modeling" section and

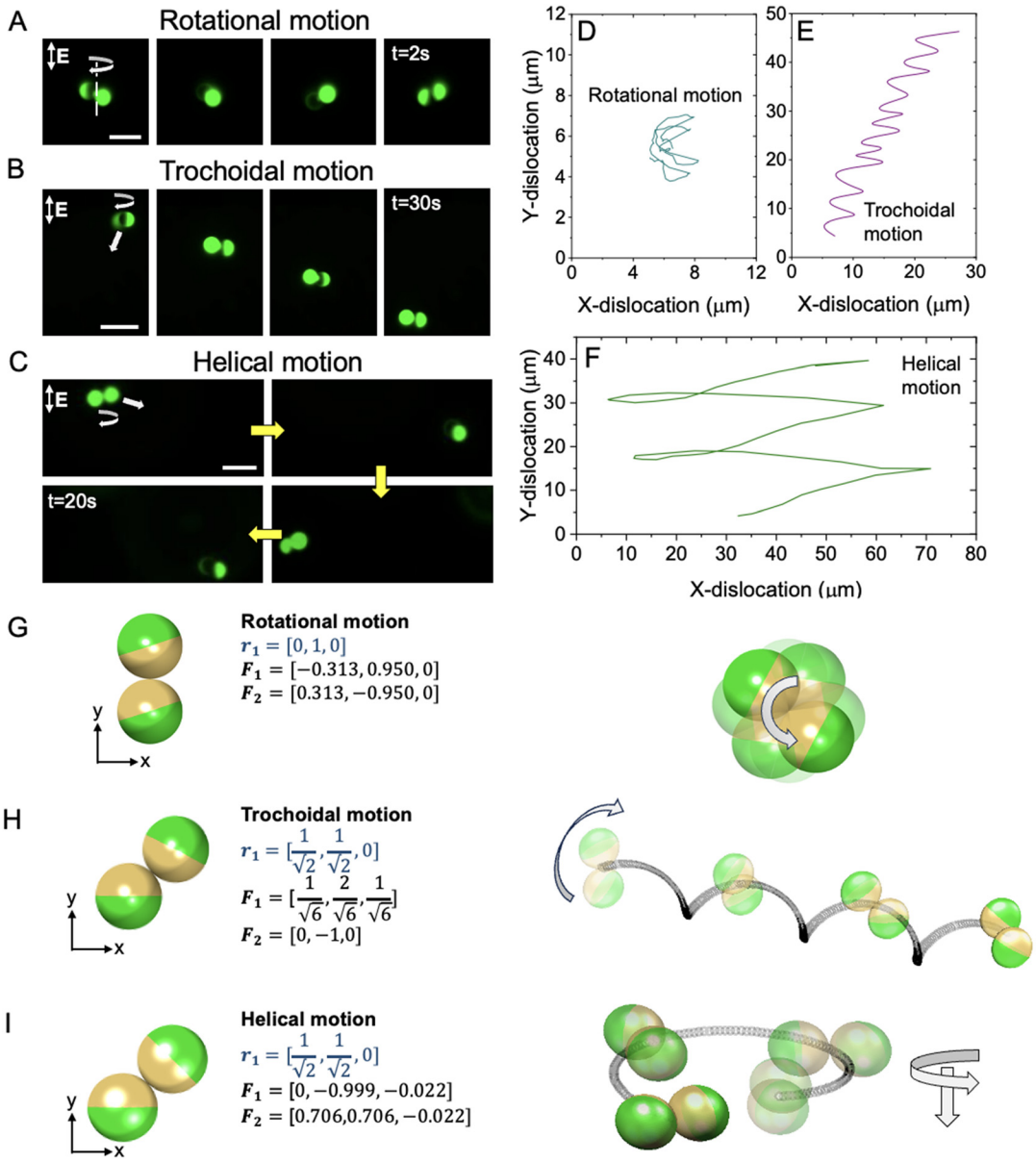

Fig. 3 Janus particle dimers exhibiting rotational, trochoidal, and helical motions. (A–C) Time-lapse images of experimentally observed dimers exhibiting (A) rotational, (B) trochoidal, and (C) helical motions, captured *via* fluorescence microscopy. (D–F) Plotted particle trajectory for (D) rotational, (E) trochoidal, and (F) helical motions extracted from the particle tracking videos used to generate the time-lapse images in (A), (B), and (C), respectively. (G–I) Schematic illustrations of the approximate configurations of the dimers and position vectors as well as trajectories of the clusters in (A), (B), and (C), respectively, as simulated using a rigid beads model. Scale bars in (A), (B), and (C) = 10 μm.

Published on 02 Nhlangula 2023. Downloaded on 2025-09-02 21:37:52.

the ESI†). Using this model, we generated theoretical trajectories of this dimer configuration and found qualitative agreement between theory and experiments (Fig. 2E), wherein the dimer cluster experienced linear translation toward the PS hemispheres.

To further evaluate the distinct types of motions exhibited in this system and further verify predictions by our model, we isolated and captured videos of dimeric clusters that exhibited rotational (Fig. 3A and Movie S2†), trochoidal (Fig. 3B and Fig. S5, Movie S3†), and helical motions (Fig. 3C and Fig. S6, Movie S4†). We define rotational motion as the spinning of clusters about their common origin (*i.e.*, close to or in line with their point of contact) and helical motion as the orbit of clusters around a central point outside of the dimer while undergoing translation. Last, we define trochoidal motion as concurrent rotational and translational motion. The tracked experimental trajectories of clusters exhibiting rotational, trochoidal, and helical motions are shown in Fig. 3D, E and F, respectively. We analyzed videos to determine the approximate relative orientations of particles within a cluster; following this, we generated theoretical trajectories for each of these clusters using the previously described rigid beads model (Fig. 3G, H and I). Again, we found strong qualitative agreement between the character of the trajectories predicted by the model and those observed experimentally. It may be expected that the proximity of particles in a dimer or other cluster configuration would lead to disruption of the electroosmotic flows over the particles, therefore impacting particle trajectories;[41] however, this was noted and addressed by Wu *et al.*, where these perturbations were modeled through a first-order method of reflections.[53] In essence, each constituent bead moves due to the external electric field along with the entrained electrohydrodynamic flow of the other bead as a first-order correction. While qualitatively similar to the beads modeling technique applied in our analysis, our methodology captures corrections beyond the first order and is hydrodynamically more precise for a pair of touching spheres than Wu *et al.* In contrast, the force calculations in our model are only accurate up to the leading order, where the net forces and torques are the sum of the electric forces independently acting on each particle. Hence, we do not capture the perturbation in force on a particle due to the presence of the other. This perturbation being a higher-order effect is not necessary to qualitatively predict the motion of our clusters,[54] as seen in Fig. 2E and 3G–I. Indeed, the qualitative agreement between the four distinct observed and predicted motions (*i.e.*, translational, rotational, trochoidal, and helical) suggests that the simplified effective net forces normal to the patch hemispheres are sufficient for model-based, qualitative prediction of the character of complex motions arising from slight changes to the relative orientations of Janus particles in a dimeric cluster.

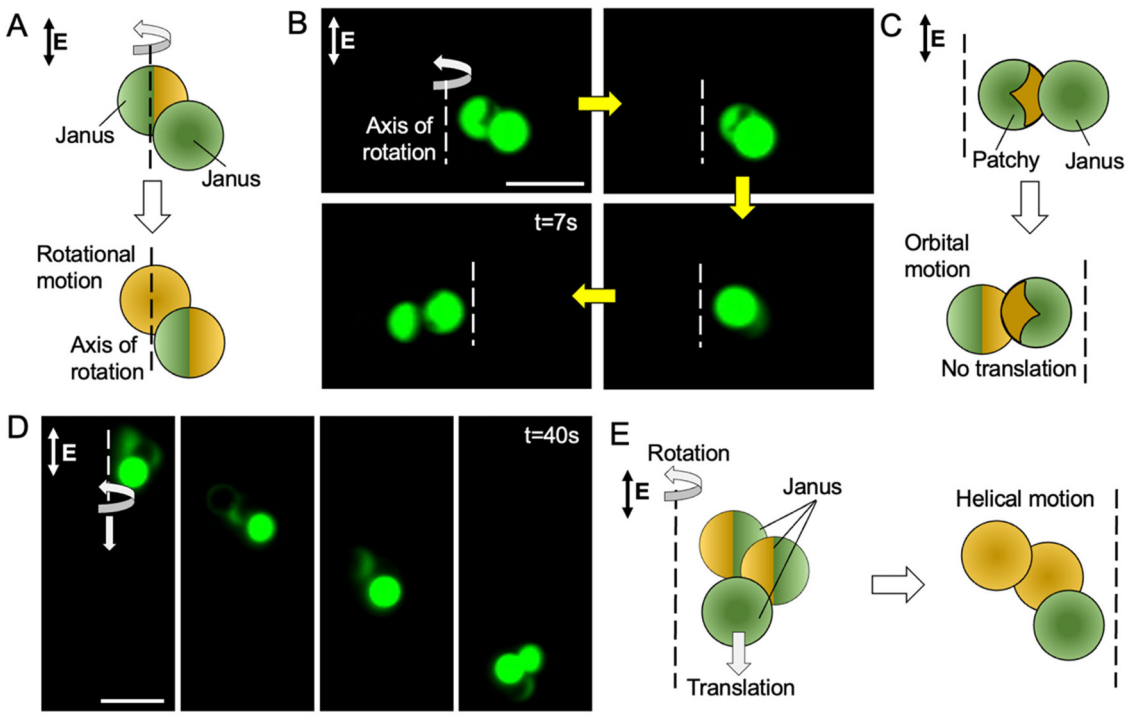

Fig. 4 Patchy particle dimers and Janus particle trimers exhibiting orbital and complex helical motions. (A) Schematic illustration showing rotational motion of a Janus–Janus particle cluster (Fig. 3A). (B) Time-lapse images of an experimentally observed Janus patchy particle cluster exhibiting an orbital motion, captured *via* fluorescence microscopy. (C) Schematic illustration showing orbital motion of a patchy–Janus particle cluster. (D) Time-lapse images of an experimentally observed a trimeric cluster exhibiting helical motion, captured *via* fluorescence microscopy. (E) Schematic illustration showing helical motion of a trimeric cluster. Scale bars in (A) and (D) = 10 μm.

 This journal is © The Royal Society of Chemistry 2023

Published on 02 Nhlangula 2023. Downloaded on 2025-09-02 21:37:52.

In addition to dimers, this system spontaneously generates more complex clusters, including trimers, tetramers, *etc.*, each displaying unique motions. To continue exploring the richness of this system, we examined the motion of dimers consisting of both patchy and Janus particles as well as trimeric clusters. To fabricate patchy particles, we used glancing angle deposition of the metallic layers described earlier to form non-hemispherical patches (Fig. S7†). Using these particles, we first examined a dimer cluster consisting of a Janus particle and a patchy particle with a triangular patch. Compared the propulsion of a dimer formed from two Janus particles, which rotates about an axis found within the cluster (Fig. 3A and 4A), we observed that a dimer formed from Janus particle and a patchy particle rotates about an axis that is outside of the cluster (Fig. 4B, C and Movie S5†). This orbital motion may be attributed to a combination of the orbital component of the motion of the patchy particle, which is known to be a three-dimensional helix,[37,55] and the linear translational motion of the Janus particle. When combined, the translational motion of the Janus particle of the dimer counteracts the translational motion of the patchy particle along the *Z*-direction, thus preventing helical motion along the *Z*-direction.

As previously described, we observed several trimeric clusters with numerous configurations. A rigorous study of these more complex clusters is reserved for future work; however, we studied one trimer configuration that exhibited helical motion (Fig. 4D and Movie S5†). Upon extracting the geometric orientation of the particles, we observed that the effective forces on the patches of individual spherical particles in the assembly appear to be the primary contributors to the experimentally observed direction of orbit along the helical path (Fig. 4E). This example highlights the ability to access various regimes of motion with multiparticle micromotor clusters, which may be useful for the development of micromotors capable of performing complex tasks such as transporting and manipulating high-value cargo.

Conclusions

We show a simple system that leverages magnetic locking of metallodielectric particles into clusters of varied configurations to experimentally explore a range of particle trajectories in a single experiment. We further demonstrate that a rigid beads model qualitatively aligns with the experimentally observed, complex motions of various configurations of dimeric clusters. This suggests that electrohydrodynamic interactions between particles does not play a substantial role in cluster motion, but the summed forces due to ICEP normal to the metallic patch of each particle dominate in the case of the dimers studied.

The presented system could enable the future design of electrokinetic micromotors. By predicting the trajectories of specific cluster configurations, it becomes possible to design particle assemblies to accomplish specific tasks. In this system, the assembly of particles into distinct dimeric and trimeric clusters through magnetic locking is predominantly random. However, by leveraging techniques such as glancing angle deposition of the magnetic patch,[37,44,56] templating magnetic patches onto micromotors,[57–59] or directing the assembly of magnetic particles after application of the electric field, researchers can create particles that predictably assemble and self-limit to a desired cluster configuration to access a prescribed regime of motion and accomplish a specific task. For example, by depositing magnetic patches much smaller than one hemisphere, therefore reducing the number of possible cluster configurations, particles could be programmed to form consistent clusters to reliably exhibit one or more of the trajectories revealed in this study. If combined with other technologies, such as the ability to carry other particles, cells, or molecules, these programmed clusters could be used to deliver rare or high-value cargo through complex 3D environments.

Experimental section

Janus particle preparation

Janus particles were prepared by e-beam evaporation of Cr, Co, and Au onto a submonolayer of 5.1 μm green or red fluorescent PS particles (Magsphere). To prepare the submonolayers, a convective assembly-inspired approach was used.[60] Specifically, two borosilicate glass slides were cleaned and dried with acetone (Millipore Sigma). The substrate slide was attached horizontally to the immobile end of a GenieTouch syringe pump (Kent Scientific), while the deposition slide was attached to the mobile syringe holder connected to the drive-shaft. The deposition slide was brought into contact with the substrate slide at a ~45° angle. The particles were washed three to four times into Milli-Q water (MQW) to remove surfactants and the solution was concentrated to 10 wt%. After briefly sonicating, 10 μL of the particle solution was pipetted onto the substrate slide at the point of contact with the deposition slide, forming a thin, uniform line of particle solution across the contact line between the slides. The syringe pump was calibrated to a 30 mL Becton Dickinson syringe and set to the full position. Then, the pump was engaged, and the deposition slide was pushed across the substrate slide at a rate of 2.5 mL min^{-1} until the deposited particle solution was exhausted. This occurred approximately halfway across the deposition slide when the pump indicated an ejected volume of ~13 mL. The deposition slide was then cleaned to prevent particle buildup, and the slides were once again brought into contact slightly past where the previous particle deposition ended. This procedure was repeated to fill the slide. To fabricate non-magnetic Janus particles, slides with submonolayers were then coated with 10 nm Cr for enhanced metal patch adhesion and 30 nm Au using an electron-beam evaporator (Edwards Auto 306 Cryo). To fabricate magnetic Janus particles, slides with submonolayers were instead coated with 10 nm Cr, 10 nm Co, and 30 nm Au. Coated particles were removed from the slides by gently scraping with a metal spatula, resuspended in MQW, and transferred to a microcen-

Published on 02 Nhlangula 2023. Downloaded on 2025-09-02 21:37:52.

trifuge tube for storage. The particles were then sonicated for ~30 s to separate aggregates.

Patchy particle preparation

For fabrication of particles with triangular patches (*i.e.*, patchy particles), the same PS particles were deposited on a glass slide *via* a Langmuir–Blodgett trough (NIMA). Briefly, 1 mL of a 5 wt% solution of PS spheres dispersed in a 50 vol% aqueous ethanol solution was carefully sprayed at the air–water interface of a trough filled with MQW using a pipette. The particles were deposited on a substrate at a surface pressure of 22 mN m^{-1} to form a closed-pack monolayer of a colloidal crystal (Fig. S7†). The triangular metal patch was introduced on the PS particles by glancing angle deposition (angle between the substrate and the incident metal vapor = 10°), and the substrate was transferred to an e-beam deposition chamber.[43,44,61] The metal deposition on the particles was performed identically to that described for the preparation of magnetic Janus particles.

Coplanar propulsion chamber fabrication

To fabricate coplanar propulsion chambers, borosilicate glass slides were masked with a ~2 mm adhesive Kapton tape mask that covered the length of the slides. Then 20 nm Cr and 100 nm Au were deposited on the masked slides by e-beam evaporation. After removal of the mask, the roughly 2 mm uncoated gap in the center of the slide (along its length) remained, with two electrodes on either side. Two strips of Cu tape were adhered to the top of the Au electrodes to form connection points for electrical leads. Additional details on the fabrication and use of the propulsion chamber are available in the ESI.†

ICEP propulsion experiments

The coplanar propulsion chambers were washed thoroughly with acetone before each experiment. A hydrophobic barrier pen (IHC World) was used to draw a roughly 1.25 cm × 1.25 cm square outline that overlapped with both electrodes. Two pieces of PTFE tape (RS Crum & Company) were placed flat and perpendicular to the electrodes at the boarder of the hydrophobic boundary. Then 10–20 μL of Janus particle cluster samples were pipetted onto the small space left between the PTFE tape spacers and the Au electrodes, and a coverslip was placed over the spacers. Then the entire chamber was placed on a Zeiss AxioVert A1 TL/RL inverted fluorescence microscope equipped with a Axiocam 305 mono camera (Zeiss, Germany). An Agilent 33210A waveform generator (Agilent) was attached to a Tegam 2340 high voltage amplifier (Tegam), and electrical leads from the amplifier were attached to the Cu tape on the propulsion chamber. A 4 kHz square wave signal was generated, amplified, and applied to the propulsion chamber, forming an electric field with magnitudes of ~750 V cm^{-1}. Resultant cluster motion was observed and recorded using the microscope camera, typically in fluorescence mode, using a 120 W mercury lamp (Excelitas) and a 545/25 nm excitation filter and a 605/70 nm emission filter or a 470/40 nm excitation filter and a 525/50 nm emission filter (Zeiss).

Video processing

Videos of clusters undergoing ICEP captured during experiments were analyzed using ImageJ software.[62] Videos were exported as AVI files while maintaining the native micron/pixel ratio and relative time information. All color correction, cropping, and time-lapse image overlay generation was completed using standard ImageJ functions. To track particles and extract position information, the "analyze particles" feature was used.

Janus assembly propulsion modeling

To model the presented Janus assemblies, we used a rigid beads model driven by an effective force on the particle.[63] The rigid beads model is able to capture hydrodynamic interactions in multiparticle assemblies comprising two or more particles. In this model, the effective force acting on each individual particle has not been mechanistically derived. A detailed derivation can be found elsewhere in literature.[54,64,65]

As stated previously in ICEP literature,[48,64,65] the inward electroosmotic flow around the particle is enhanced on the side of the more polarizable surface. Our model qualitatively captures this effect by considering an outward, constant force directed symmetrically through the centroid of the metallic patch of each individual spherical particle in the assembly. The magnitude of the force is estimated from scaling estimates from the results of Squires and Bazant.[65] For spherical Janus particles with hemispherical caps, the translation velocity is $U_{\mathrm{ICEP}} \sim 3RE^2/32\eta$. Assuming that only the hydrodynamic drag and the force due to the induced charge asymmetry are acting on the body. Hence, the effective force on the sphere is $F_{\mathrm{ICEP}} \sim 18\pi R^2E^2/32$. Utilizing U_{ICEP} and F_{ICEP} to scale the velocity and force in our calculations, we consider a non-dimensional force of magnitude one acting through the centroid of the patch.

Additional information on obtaining the particle velocity and trajectory for a general dimeric configuration is available in the ESI.†

Author contributions

This manuscript was written through contributions of all authors, and all authors have given final approval to the final version of the manuscript.

Conflicts of interest

There are no conflicts to declare.

Acknowledgements

The authors thank to Prof. Daniel Schwartz (CU Boulder) for the use of the Langmuir–Blodgett trough. This work was primarily funded by a National Science Foundation (NSF)

 This journal is © The Royal Society of Chemistry 2023

Published on 02 Nhlangula 2023. Downloaded on 2025-09-02 21:37:52.

CAREER grant (CBET 2143419). C. W. S. is a Pew Scholar in the Biomedical Sciences, supported by the Pew Charitable Trusts. C. W. S. would also like to thank the Packard Foundation for their support of this project. Additional support from the National Institutes of Health (NIH R21AI154266) and the U.S. Department of Education Graduate Assistantships in Areas of National Need (GAANN) Program for Soft materials (ED P200A180070) is acknowledged.

References

1 H. Lee, D. Kim, S. Kwon and S. Park, *ACS Appl. Mater. Interfaces*, 2021, **13**, 19633–19647.
2 J. G. Lee, R. R. Raj, C. P. Thome, N. B. Day, P. Martinez, N. Bottenus, A. Gupta and C. W. Shields, *Small*, 2023, **19**, 2300409.
3 Y. Gao, B. Sprinkle, E. Springer, D. W. M. Marr and N. Wu, *Sci. Adv.*, 2023, **9**, eadg0919.
4 J. G. Lee, R. R. Raj, N. B. Day and C. W. Shields, *ACS Nano*, 2023, **17**, 14196–14204.
5 M. Medina-Sánchez, L. Schwarz, A. K. Meyer, F. Hebenstreit and O. G. Schmidt, *Nano Lett.*, 2016, **16**, 555–561.
6 Z. Lin, X. Fan, M. Sun, C. Gao, Q. He and H. Xie, *ACS Nano*, 2018, **12**, 2539–2545.
7 C. W. Shields, *Acc. Mater. Res.*, 2023, **4**, 566–569.
8 S.-N. Yin, C.-F. Wang, Z.-Y. Yu, J. Wang, S.-S. Liu and S. Chen, *Adv. Mater.*, 2011, **23**, 2915–2919.
9 Y. Shi, X. Zhou and G. Yu, *Acc. Chem. Res.*, 2017, **50**, 2642–2652.
10 Y. Sun, M. Yang, Y. Guo, M. Cheng, B. Dong and F. Shi, *Angew. Chem., Int. Ed.*, 2020, **59**, 1098–1102.
11 A. M. Boymelgreen, T. Balli, T. Miloh and G. Yossifon, *Nat. Commun.*, 2018, **9**, 760.
12 S. Ghosh and A. Ghosh, *Nat. Commun.*, 2019, **10**, 4191.
13 D. Lyu, W. Xu, N. Zhou, W. Duan, Z. Wang, Y. Mu, R. Zhou and Y. Wang, *Sci. Adv.*, 2023, **9**, eadh2250.
14 D. Jin, Q. Wang, K. F. Chan, N. Xia, H. Yang, Q. Wang, S. C. H. Yu and L. Zhang, *Sci. Adv.*, 2023, **9**, eadf9278.
15 Y. Yang and M. A. Bevan, *Sci. Adv.*, 2020, **6**, eaay7679.
16 M. B. Akolpoglu, Y. Alapan, N. O. Dogan, S. F. Baltaci, O. Yasa, G. Aybar Tural and M. Sitti, *Sci. Adv.*, 2022, **8**, eabo6163.
17 C. C. J. Alcântara, S. Kim, S. Lee, B. Jang, P. Thakolkaran, J.-Y. Kim, H. Choi, B. J. Nelson and S. Pané, *Small*, 2019, **15**, 1805006.
18 R. Maria-Hormigos, C. C. Mayorga-Martinez and M. Pumera, *Small*, 2022, 2204887.
19 Y. Hou, H. Wang, R. Fu, X. Wang, J. Yu, S. Zhang, Q. Huang, Y. Sun and T. Fukuda, *Lab Chip*, 2023, **23**, 848–868.
20 L. O. Mair, B. A. Evans, A. Nacev, P. Y. Stepanov, R. Hilaman, S. Chowdhury, S. Jafari, W. Wang, B. Shapiro and I. N. Weinberg, *Nanoscale*, 2017, **9**, 3375–3381.
21 H. Ye, Y. Wang, X. Liu, D. Xu, H. Yuan, H. Sun, S. Wang and X. Ma, *J. Colloid Interface Sci.*, 2021, **588**, 510–521.
22 J.-F. Louf, N. Bertin, B. Dollet, O. Stephan and P. Marmottant, *Adv. Mater. Interfaces*, 2018, **5**, 1800425.
23 A. Aghakhani, O. Yasa, P. Wrede and M. Sitti, *Proc. Natl. Acad. Sci. U. S. A.*, 2020, **117**, 3469–3477.
24 T. B. Alina, H. B. Kirkpatrick, N. M. Bower, S. D. Curry, T. R. Ausec, S. A. Saemundsson, E. N. Mueller, C. W. Shields, J. N. Cha and A. P. Goodwin, *ACS Appl. Nano Mater.*, 2023, **6**, 13720–13729.
25 C. P. Thome, W. S. Hoertdoerfer, J. R. Bendorf, J. G. Lee and C. W. I. Shields, *Nano Lett.*, 2023, **23**, 2379–2387.
26 Y. Dou, C. A. Cartier, W. Fei, S. Pandey, S. Razavi, I. Kretzschmar and K. J. M. Bishop, *Langmuir*, 2016, **32**, 13167–13173.
27 G. Kokot, H. A. Faizi, G. E. Pradillo, A. Snezhko and P. M. Vlahovska, *Commun. Phys.*, 2022, **5**, 91.
28 X. Zhu, Y. Gao, R. Mhana, T. Yang, B. L. Hanson, X. Yang, J. Gong and N. Wu, *Langmuir*, 2021, **37**, 9151–9161.
29 J. Wu, S. Balasubramanian, D. Kagan, K. M. Manesh, S. Campuzano and J. Wang, *Nat. Commun.*, 2010, **1**, 36.
30 B. Jurado-Sánchez, M. Pacheco, J. Rojo and A. Escarpa, *Angew. Chem., Int. Ed.*, 2017, **56**, 6957–6961.
31 B. Landry, V. Girgis and J. G. Gibbs, *Small*, 2020, **16**, 2003375.
32 L. Soler and S. Sánchez, *Nanoscale*, 2014, **6**, 7175–7182.
33 D. Li, Y. Liu, Y. Yang and Y. Shen, *Nanoscale*, 2018, **10**, 19673–19677.
34 C. W. Shields IV, K. Han, F. Ma, T. Miloh, G. Yossifon and O. D. Velev, *Adv. Funct. Mater.*, 2018, **28**, 1803465.
35 A. M. Brooks, S. Sabrina and K. J. M. Bishop, *Proc. Natl. Acad. Sci. U. S. A.*, 2018, **115**, E1090–E1099.
36 N. Jarvey, F. Henrique and A. Gupta, *Soft Matter*, 2023, **19**, 6032–6045.
37 J. G. Lee, A. M. Brooks, W. A. Shelton, K. J. M. Bishop and B. Bharti, *Nat. Commun.*, 2019, **10**, 2575.
38 Z. Wang, Z. Wang, J. Li, S. T. H. Cheung, C. Tian, S.-H. Kim, G.-R. Yi, E. Ducrot and Y. Wang, *J. Am. Chem. Soc.*, 2019, **141**, 14853–14863.
39 J. G. Lee, A. Al Harraq, K. J. M. Bishop and B. Bharti, *J. Phys. Chem. B*, 2021, **125**, 4232–4240.
40 K. J. M. Bishop, S. L. Biswal and B. Bharti, *Annu. Rev. Chem. Biomol. Eng.*, 2023, **14**, 1–30.
41 A. Boymelgreen, G. Yossifon, S. Park and T. Miloh, *Phys. Rev. E: Stat., Nonlinear, Soft Matter Phys.*, 2014, **89**, 011003.
42 S. Ebbens, R. A. L. Jones, A. J. Ryan, R. Golestanian and J. R. Howse, *Phys. Rev. E: Stat., Nonlinear, Soft Matter Phys.*, 2010, **82**, 015304.
43 A. B. Pawar and I. Kretzschmar, *Macromol. Rapid Commun.*, 2010, **31**, 150–168.
44 A. B. Pawar and I. Kretzschmar, *Langmuir*, 2009, **25**, 9057–9063.
45 A. A. Harraq, B. D. Choudhury and B. Bharti, *Langmuir*, 2022, **38**, 3001–3016.
46 S. Gangwal, O. J. Cayre, M. Z. Bazant and O. D. Velev, *Phys. Rev. Lett.*, 2008, **100**, 058302.
47 K. Han, *Micromachines*, 2023, **14**, 661.

Published on 02 Nhlangula 2023. Downloaded on 2025-09-02 21:37:52.

48 M. Z. Bazant and T. M. Squires, *Phys. Rev. Lett.*, 2004, **92**, 066101.
49 N. M. Diwakar, G. Kunti, T. Miloh, G. Yossifon and O. D. Velev, *Curr. Opin. Colloid Interface Sci.*, 2022, **59**, 101586.
50 A. M. Boymelgreen, G. Kunti, P. Garcia-Sanchez, A. Ramos, G. Yossifon and T. Miloh, *J. Colloid Interface Sci.*, 2022, **616**, 465–475.
51 C. Peng, I. Lazo, S. V. Shiyanovskii and O. D. Lavrentovich, *Phys. Rev. E: Stat., Nonlinear, Soft Matter Phys.*, 2014, **90**, 051002.
52 S. Gangwal, O. J. Cayre and O. D. Velev, *Langmuir*, 2008, **24**, 13312–13320.
53 F. Ma, X. Yang, H. Zhao and N. Wu, *Phys. Rev. Lett.*, 2015, **115**, 208302.
54 A. Ganguly and A. Gupta, *Phys. Rev. Fluids*, 2023, **8**, 014103.
55 A. Al Harraq, M. Bello and B. Bharti, *Curr. Opin. Colloid Interface Sci.*, 2022, **61**, 101612.
56 R. J. Archer, A. I. Campbell and S. J. Ebbens, *Soft Matter*, 2015, **11**, 6872–6880.
57 K. Han, C. W. Shields, B. Bharti, P. E. Arratia and O. D. Velev, *Langmuir*, 2020, **36**, 7148–7154.
58 S. Puce, E. Sciurti, F. Rizzi, B. Spagnolo, A. Qualtieri, M. De Vittorio and U. Staufer, *Micro Nano Eng.*, 2019, **2**, 70–75.
59 G. Zabow, *Science*, 2022, **378**, 894–898.
60 B. G. Prevo, D. M. Kuncicky and O. D. Velev, *Colloids Surf., A*, 2007, **311**, 2–10.
61 A. Al Harraq, J. G. Lee and B. Bharti, *Sci. Adv.*, 2020, **6**, eaba5337.
62 W. Wang and T. E. Mallouk, *ACS Nano*, 2021, **15**, 15446–15460.
63 P. J. Zuk, B. Cichocki and P. Szymczak, *Biophys. J.*, 2018, **115**, 782–800.
64 T. M. Squires and M. Z. Bazant, *J. Fluid Mech.*, 2004, **509**, 217–252.
65 T. M. Squires and M. Z. Bazant, *J. Fluid Mech.*, 2006, **560**, 65.

This journal is © The Royal Society of Chemistry 2023